

Charge Pumping Induced by Magnetic Texture Dynamics in Weyl Semimetals

著者	Yasufumi Araki, Kentaro Nomura
journal or publication title	PHYSICAL REVIEW APPLIED
volume	10
number	014007
page range	1-7
year	2018-07-11
URL	http://hdl.handle.net/10097/00125361


doi: 10.1103/PhysRevApplied.10.014007

Charge Pumping Induced by Magnetic Texture Dynamics in Weyl Semimetals

Yasufumi Araki^{1,2,*} and Kentaro Nomura¹

¹*Institute for Materials Research, Tohoku University, Sendai 980–8577, Japan*

²*Frontier Research Institute for Interdisciplinary Sciences, Tohoku University, Sendai 980–8578, Japan*

 (Received 8 November 2017; revised manuscript received 16 March 2018; published 11 July 2018)

Spin-momentum locking in Weyl semimetals correlates the orbital motion of electrons with background magnetic textures. We show here that the dynamics of a magnetic texture in a magnetic Weyl semimetal induces a pumped electric current that is free from Joule heating. This pumped current can be regarded as a Hall current induced by axial electromagnetic fields equivalent to the magnetic texture. Taking a magnetic domain wall as a test case, we demonstrate that a moving domain wall generates a pumping current corresponding to the localized charge.

DOI: [10.1103/PhysRevApplied.10.014007](https://doi.org/10.1103/PhysRevApplied.10.014007)

I. INTRODUCTION

Magnetic textures, such as domain walls (DWs), skyrmions, spin spirals, etc., are currently attracting a great deal of interest in condensed matter physics. In the context of spintronics, these magnetic textures are expected to assume an integral role as information carriers in next-generation devices and in switching devices driven by electric and spin currents [1–3]. In particular, the dynamical properties of such magnetic textures, which are coupled to the spins of conduction electrons, are the focus of intense efforts to control and detect them efficiently, and promise a wide range of future applications [4]. Depending on the particular context, different dynamical perspectives can be used to describe the coupling between magnetic textures and conduction electrons. One may view the spin-transfer torque arising from the spins of conduction electrons as primarily responsible for driving the dynamics of magnetic textures [5], or conversely, see the dynamics of a magnetic texture as inducing an external force on conduction electrons through changes in the electron Berry phase, which is known as the spin motive force [6].

In this work, we propose that the dynamics of magnetic textures in Weyl semimetals (WSMs) can invoke electric charge pumping free from backscattering in a manner that is distinct from that induced by the spin motive force. WSMs form a class of topological materials characterized by a conical band structure and pair(s) of band-touching points (Weyl points) isolated from each other in the bulk Brillouin zone [7–10]. This “Weyl cone” structure arises from band inversion due to strong spin-orbit coupling (SOC), and is associated with significant electron spin-momentum locking around the nodal points.

For such spin-momentum-locked electrons, the exchange coupling to the background magnetic texture is analogous to a fictitious vector potential, which is referred to as an “axial vector potential” [11]. In the context of this analogy, we can then observe a “Hall current” free from Joule heating that is induced by the axial magnetic and electric fields corresponding to the dynamics of the background magnetic texture. This “Hall effect” accounts for the charge-pumping mechanism proposed here.

Recent studies that experimentally synthesized and observed magnetic WSM phases open a new way of designing future spintronic devices based on WSMs [12, 13]. The significance of magnetic textures in WSMs is discussed in several recent studies. Based on the features of the electron spin-momentum locking, it was proposed in the previous papers that the correlation between the magnetic moments (mediated by the Weyl electrons) exhibits longitudinal anisotropy, distinguishing it from that due to ordinary isotropic Ruderman-Kittel-Kasuya-Yosida (RKKY) interactions [14–16]. Such anisotropic correlations then give rise to the formation of nontrivial topological magnetic textures in WSMs. Moreover, once a magnetic DW is formed in a WSM, it is accompanied by a certain amount of electric charge and an equilibrium current localized to the DW, no matter how the DW is introduced into the WSM [17, 18]. While the theories proposed in these studies principally account for the characteristics of static magnetic textures in WSMs, the dynamical properties of magnetic textures in WSMs are much less understood and a better understanding of such properties is required for the ability to read and write information in future devices. The charge-pumping effect discussed in this work is one such dynamical property attributed to magnetic textures in WSMs. Moreover, since it arises as a Hall current due to axial electromagnetic fields, it is

*araki@imr.tohoku.ac.jp

free from Joule heating and could lead to reduced power consumption in future spintronic applications.

II. WEYL HAMILTONIAN AND AXIAL GAUGE FIELDS

The formation of the WSM phase requires the breaking of either time-reversal symmetry (TRS) or spatial inversion symmetry so that the degeneracy of the Weyl cones is lifted. TRS breaking in WSMs is typically realized by the introduction of magnetic order in the system. Weyl semimetallic phases with magnetic orders are predicted theoretically in various Co- and Mn-based alloys, based on the tight-binding model and first-principle calculations [19–23]. Some of them are experimentally realized in the latest studies, such as the WSM phase with (i) ferromagnetism in the Heusler alloy $\text{Co}_3\text{Sn}_2\text{S}_2$ (Ref. [12]) and (ii) noncollinear antiferromagnetism in Mn_3Sn (Ref. [13]), in both of which the electron transport properties are now being intensely measured. The breaking of TRS shifts the positions of the Weyl nodes in momentum space, and this effect can be regarded as a “emergent vector potential” for each Weyl node [11]. As far as the low-energy phenomena are concerned, one can then rely on this idea of an effective vector potential to treat the temporal and spatial variations of the magnetization in the system more efficiently.

Here, we consider a minimal model of a WSM exhibiting ferromagnetic order, with a pair of Weyl cones dispersed isotropically around each Weyl node. If we require cubic symmetry, the electron momentum $\mathbf{p} = -i\nabla$ and its spin $\boldsymbol{\sigma} = (\sigma_x, \sigma_y, \sigma_z)$ are locked with each other around the Weyl points, with $\boldsymbol{\sigma}$ the Pauli matrices, since the band crossing arises from atomic spin-orbit coupling. There we can rely on the minimal continuum Hamiltonian

$$\mathcal{H} = sv_F(\mathbf{p} \cdot \boldsymbol{\sigma}) - J\mathbf{M}(\mathbf{r}, t) \cdot \boldsymbol{\sigma}, \quad (1)$$

at low energy (around the Weyl points), with $s = \pm$ denoting the chirality of each Weyl node and v_F the Fermi velocity. For convenience, we take $\hbar = 1$ here. The second term in this Hamiltonian describes the exchange coupling between the electron spin $\boldsymbol{\sigma}$ and the local magnetic texture $\mathbf{M}(\mathbf{r}, t)$, with coupling constant J . Then, provided that our Weyl-cone approximation is valid, the local magnetic texture $\mathbf{M}(\mathbf{r}, t)$ can be viewed as a U(1) axial gauge potential $A_5(\mathbf{r}, t) = (J/v_F e)\mathbf{M}(\mathbf{r}, t)$ coupled to the electrons, and in terms of which our Hamiltonian can be written as

$$\mathcal{H} = sv_F[\mathbf{p} - se\mathbf{A}_5(\mathbf{r}, t)] \cdot \boldsymbol{\sigma}. \quad (2)$$

In contrast to a normal vector potential \mathbf{A} , the axial vector potential \mathbf{A}_5 couples to different chirality modes ($s = \pm$) with opposite sign and is not subject to Maxwell’s equations. It is known that the axial gauge potential can

also describe the effect of lattice strain in Dirac semimetals Na_3Bi and Cd_3As_2 (see Ref. [24]). While the strain-induced gauge field is restricted by the stiffness of the crystal, one can generate a variety of field structures from the background magnetic textures in our case.

As we show in the following sections (and by analogy to normal vector potentials), it is this axial vector potential that is responsible for the proposed electron transport. We take the Fermi level μ close to the Weyl nodes, so that the electrons contributing to the charge transport can be well described by this low-energy Hamiltonian. We assume here that there are no other metallic bands crossing the Fermi level, otherwise they may give additive contribution to the charge transport and may obscure the characteristic behavior in WSMs discussed below.

It should be noted that this axial gauge potential is distinct from the emergent gauge potential that arises at magnetic textures in metals or semiconductors with topologically trivial band structures [25–27]: the emergent gauge potential comes from the real-space Berry connection and thus depends only on the relative angle between neighboring spins, whereas the axial gauge potential \mathbf{A}_5 in WSM depends on the direction of the background magnetization \mathbf{M} itself. Therefore, we may expect richer phenomena arising from magnetic textures in WSMs, compared with topologically trivial electron systems. For instance, while Néel and Bloch DWs give the same emergent gauge field structure for trivial electrons, they yield different axial gauge field structures for Weyl electrons and thus lead to quantitatively different charge-pumping behavior, as we note in Sec. IV.

III. FIELD-INDUCED CURRENT AND CHARGE PUMPING

Before considering the proposed charge-pumping mechanism, let us first review the different kinds of electric current induced by real EMFs. Currents induced by EMFs in a WSM can be classified based on their linear response to an electric field \mathbf{E} and/or magnetic field \mathbf{B} (see Table I). If only an \mathbf{E} field is applied to the WSM, a longitudinal drift current, $\mathbf{j}^{(D)} = \sigma_D \mathbf{E}$, is induced, where σ_D is the longitudinal conductivity of a pair of Weyl cones. If TRS is broken in the WSM by the presence of magnetization \mathbf{M} , an anomalous Hall effect (AHE) is also present [28–31], and drives the transverse current $\mathbf{j}^{(A)} = \sigma_A \hat{\mathbf{M}} \times \mathbf{E}$, where the anomalous Hall conductivity is given by $\sigma_A = (e/2\pi^2)(J|\mathbf{M}|/v_F)$ [32].

On the other hand, if only a magnetic field \mathbf{B} is applied to the system, it induces Landau quantization with a cyclotron frequency $\omega_c = v_F \sqrt{2eB}$. Nonzero Landau levels (LLs) then appear symmetrically about the zero energy due to particle-hole symmetry, and the zeroth LL is linearly dispersed along the magnetic field. As the dispersion direction

TABLE I. Classification of currents induced by normal and axial electromagnetic fields (EMFs). The current induced by axial EMFs is evaluated with $\mu_5 = 0$.

	Normal EMFs (\mathbf{E}, \mathbf{B})	Axial EMFs ($\mathbf{E}_5, \mathbf{B}_5$)
Drift	$\mathbf{j}^{(D)} = \sigma_D \mathbf{E}$	$\mathbf{j}^{(D)} = \mathbf{0}$
AHE	$\mathbf{j}^{(A)} = \sigma_A \hat{\mathbf{M}} \times \mathbf{E}$	$\mathbf{j}^{(A)} = \mathbf{0}$
CME	$\mathbf{j}^{(C)} = (e^2/2\pi^2)\mu_5 \mathbf{B}$	$\mathbf{j}^{(C)} = (e^2/2\pi^2)\mu \mathbf{B}_5$
RHE	$\mathbf{j}^{(H)} = \sigma_H \hat{\mathbf{B}} \times \mathbf{E}$	$\mathbf{j}^{(H)} = \sigma_H \hat{\mathbf{B}}_5 \times \mathbf{E}_5$

of the zeroth LL for each Weyl node depends on the chirality s [33], it only contributes to the net current $\mathbf{j}^{(C)} = (e^2/2\pi^2)\mu_5 \mathbf{B}$ if there is a chemical potential imbalance μ_5 between the two Weyl nodes. This effect is known as the chiral magnetic effect (CME) and accounts for the negative magnetoresistances observed in WSMs [28,34–37].

Finally, a combination of \mathbf{E} and \mathbf{B} induces a Hall current perpendicular to both, $\mathbf{j}^{(H)} = \sigma_H \hat{\mathbf{B}} \times \mathbf{E}$, which we have called the regular Hall effect (RHE) to distinguish it from the AHE. The regular Hall conductivity σ_H depends on both the field strength and the amount of disorder present in the system. If the level broadening arising from disorder obscures the LL spacing, i.e., if the cyclotron frequency ω_c is smaller than the relaxation rate $1/\tau$, the transport coefficients can be estimated in the classical limit using semiclassical (Boltzmann) transport theory [38]. The zero-temperature Hall conductivity is then given by $\sigma_{H(c)} = -(\tau^2 e^3 \mu / 3\pi^2) |\mathbf{B}|$ at the lowest order in \mathbf{B} , where μ is the electron chemical potential measured from the Weyl nodes. On the other hand, in the quantum limit where the disorder is dilute and the LLs can be regarded as well separated ($\omega_c \tau \gg 1$), the Hall current can be effectively described by the “quantum Hall effect”. If the Fermi level μ lies just slightly beyond the charge neutrality point so that it does not cross the higher LLs, only the zeroth LL contributes to the Hall current. The Hall conductivity then reduces to the universal value

$$\sigma_{H(q)} = \frac{e^2}{2\pi^2} \frac{\mu}{v_F}, \quad (3)$$

which can be derived from the quantum Hall conductivity in 2D Dirac systems such as graphene.

As we have mentioned above, in order to consider the effect of magnetic texture dynamics on the electron transport, we can rely on the idea of axial EMFs. Once the magnetic texture dynamics arises, it can be treated as axial EMFs for the Weyl electrons in the vicinity of the Weyl points, regardless of the origin of the magnetic texture dynamics (e.g., external magnetic field, spin-transfer torques, etc.). Specifically, the dynamics of the magnetic texture, i.e., \mathbf{r} and t dependences in the axial vector potential \mathbf{A}_5 , are equivalent to axial electric and magnetic fields,

\mathbf{E}_5 and \mathbf{B}_5 , given by

$$\mathbf{E}_5(\mathbf{r}, t) = -\partial_t \mathbf{A}_5(\mathbf{r}, t) = -\frac{J}{v_F e} \partial_t \mathbf{M}(\mathbf{r}, t), \quad (4)$$

$$\mathbf{B}_5(\mathbf{r}, t) = \nabla \times \mathbf{A}_5(\mathbf{r}, t) = \frac{J}{v_F e} \nabla \times \mathbf{M}(\mathbf{r}, t), \quad (5)$$

respectively. The electron transport induced by the magnetic texture dynamics can then be treated in terms of these axial EMFs, thus enabling its evaluation in similar fashion to normal EMFs, making the overall discussion quite simple. As we show in the following, the axial electric field \mathbf{E}_5 drives an “axial current” comprising a pair of currents flowing counter to each other at the two Weyl nodes and thus yielding no net current, while a net current is induced if it is accompanied by an axial magnetic field \mathbf{B}_5 . Here, we note that we have neglected intervalley scattering processes, so that the electron transport for each Weyl node can be treated separately.

As long as the magnetic texture dynamics are sufficiently slow and “adiabatic,” the axial electric field \mathbf{E}_5 is so weak that its nonlinear effect can be safely discarded. With this assumption, it then simply induces a drift current and an anomalous Hall current for each Weyl node flowing in opposite directions to one another, i.e., the axial current [39]. As such, it contributes no net current unless there is an imbalance in the carrier densities ($\mu_5 \neq 0$). In the quantum Hall regime of the axial magnetic field \mathbf{B}_5 , the longitudinal conductivity is ideally suppressed and hence there is no axial drift current. Although the longitudinal conductivity becomes finite in the presence of impurities, it is still tiny around the Weyl points due to the small density of states of the carriers. Therefore, Joule heating from the (axial) drift current is largely suppressed in WSMs, compared with that for topologically trivial electrons.

On the other hand, the RHE contribution is the same as that induced by normal EMFs, i.e., $\mathbf{j}^{(H)} = \sigma_H \hat{\mathbf{B}}_5 \times \mathbf{E}_5$, since both \mathbf{E}_5 and \mathbf{B}_5 couple to each chiral mode with opposite signs, driving the Hall current for each Weyl node in the same direction. As long as the disorder is weak enough compared with the level spacing, the induced Hall current can be estimated in the quantum limit in a similar fashion to the case for real \mathbf{B} and \mathbf{E} , yielding

$$\mathbf{j}^{(H)} = \frac{e^2}{2\pi^2} \frac{\mu}{v_F} \hat{\mathbf{B}}_5 \times \mathbf{E}_5, \quad (6)$$

which is independent of the field strength $|\mathbf{B}_5|$. Moreover, since the zeroth LLs of the two Weyl nodes are dispersed in the same direction along \mathbf{B}_5 [11,17,18,24], a

finite chemical potential leads to the net current

$$\mathbf{j}^{(C)} = \frac{e^2}{2\pi^2} \mu \mathbf{B}_5, \quad (7)$$

which we identify as the chiral *axial* magnetic effect (CAME), i.e., the axial counterpart of the CME [40–42]. Therefore, the total current \mathbf{j}_{ind} induced by \mathbf{E}_5 and \mathbf{B}_5 in WSMs is given (up to the linear response in \mathbf{E}_5) by the sum of $\mathbf{j}^{(H)}$ and $\mathbf{j}^{(C)}$. It should be noted that Fermi arcs may contribute to an additional conduction current on the surface, which is beyond our phenomenological analysis; we limit our analysis to the charge transport related to magnetic textures in the bulk.

We should note that typical axial EMFs arising from magnetic textures are spatially inhomogeneous. However, if the magnetic texture is sufficiently smooth over the relevant length scales (e.g., the electron’s mean free path), the axial EMFs can be regarded as “locally” uniform and we can consider the properties of the electron transport in the ballistic limit. In such cases, we can use Eqs. (6) and (7) to estimate the local current distribution. In the absence of normal EMFs \mathbf{E} and \mathbf{B} , the axial anomaly between the chiral modes (see [43–45]) does not violate the conservation of charge [11], and we can use the charge conservation relation

$$\partial_t \rho_{\text{pump}}(\mathbf{r}, t) = -\nabla \cdot \mathbf{j}_{\text{ind}}(\mathbf{r}, t), \quad (8)$$

to estimate the electric charge $\rho_{\text{pump}}(\mathbf{r}, t)$ pumped by the magnetic texture dynamics $\mathbf{M}(\mathbf{r}, t)$ via the axial field-induced current \mathbf{j}_{ind} . Since the CAME part, $\mathbf{j}^{(C)} \propto \mu(\nabla \times \mathbf{M})$, is divergence-free whenever the chemical potential is uniform, only the regular Hall current given by Eq. (6) is responsible for the ensuing charge dynamics:

$$\partial_t \rho_{\text{pump}} = \frac{e^2}{2\pi^2} \frac{\mu}{v_F} [\hat{\mathbf{B}}_5 \cdot (\nabla \times \mathbf{E}_5) - \mathbf{E}_5 \cdot (\nabla \times \hat{\mathbf{B}}_5)]. \quad (9)$$

This equation is the key result of this work, and directly relates the magnetic texture dynamics (via \mathbf{E}_5 and \mathbf{B}_5) to the pumped charge ρ_{pump} .

In order to capture this current \mathbf{j}_{ind} , or the pumped charge ρ_{pump} , one may need to attach a metallic lead to the end of the sample; once the magnetic texture jumps into the lead, it is measured as a pulse of electric current given by \mathbf{j}_{ind} . If the magnetic texture dynamics is driven by current (e.g., spin-transfer torques, spin-orbit torques), \mathbf{j}_{ind} can be captured as a current pulse localized at the magnetic texture, in addition to the driving current that is almost steady in the background. Since this current arises from the Lorentz force by the axial EMFs, the magnetic texture does not exert any work on the electrons, hence the energy dissipation from Joule heating is suppressed in the bulk. Although Joule heating is inevitable in the metallic leads, it occurs only when the current pulse enters the lead and hence it is much smaller than that from a steady current.

We note that if the spatial variation of \mathbf{M} is coplanar, the axial magnetic field \mathbf{B}_5 is uniform, i.e., $\hat{\mathbf{B}}_5$ is homogeneous over the whole system. In this case, the second term in Eq. (9) vanishes and we obtain $\partial_t \rho_{\text{pump}} = -(e^2/2\pi^2)(\mu/v_F)(\hat{\mathbf{B}}_5 \cdot \partial_t \mathbf{B}_5) = -(e^2/2\pi^2)(\mu/v_F) \partial_t |\mathbf{B}_5|$, where we have used the relation $\nabla \times \mathbf{E}_5 = \nabla \times (-\partial_t \mathbf{A}_5) = -\partial_t \mathbf{B}_5$. Thus, we obtain a further simplified relation for this restricted case

$$\rho_{\text{pump}}(\mathbf{r}, t) = -\frac{e^2}{2\pi^2} \frac{\mu}{v_F} |\mathbf{B}_5(\mathbf{r}, t)| + \text{const}, \quad (10)$$

which implies that an axial magnetic flux (i.e., the curl of the magnetization) induces localized electric charge in a WSM, irrespective of its orientation. Such a rearrangement in the charge distribution may be measured directly in thin-film geometry, e.g., by scanning tunneling microscopy (STM).

IV. EXAMPLE: MAGNETIC DOMAIN WALLS

In order to establish the validity of the relations presented above, let us consider a moving magnetic DW in a WSM as a typical example. We construct a DW of width $2w$ in the y - z plane, separating two regions of an infinite system with magnetizations $\mathbf{M}(x \rightarrow \pm\infty) = \pm M_0 \mathbf{e}_z$, and then set the DW in motion with velocity V_{DW} in the x direction by hand. The resulting magnetic texture is then given by

$$\mathbf{M}(\mathbf{r}, t) = \mathbf{M}(x - V_{\text{DW}}t) = M_0 \begin{pmatrix} \lambda_x \operatorname{sech} \xi(x, t) \\ \lambda_y \operatorname{sech} \xi(x, t) \\ \tanh \xi(x, t) \end{pmatrix}, \quad (11)$$

where $\xi(x, t) \equiv (x - V_{\text{DW}}t)/w$ denotes the relative position from the center of the DW, rescaled by the DW width. The set of parameters (λ_x, λ_y) characterizes the texture of the DW, where a DW with a coplanar magnetic texture within the x - z plane (i.e., a Néel DW) corresponds to $(\lambda_x, \lambda_y) = (\pm 1, 0)$, while a DW with a helical magnetic texture twisting in the y - z plane (i.e., a Bloch DW) is given by $(\lambda_x, \lambda_y) = (0, \pm 1)$.

In order to estimate the current \mathbf{j}_{ind} induced by the DW’s motion, we consider the axial gauge field $\mathbf{A}_5 = (J/v_F e) \mathbf{M}$. The axial EMFs are then given by

$$\mathbf{E}_5 = \frac{JV_{\text{DW}}}{ev_F w} \mathbf{M}'(\xi), \quad \mathbf{B}_5 = \frac{J}{ev_F w} \mathbf{e}_x \times \mathbf{M}'(\xi), \quad (12)$$

where $\mathbf{M}'(\xi) \equiv d\mathbf{M}(\xi)/d\xi$. The magnitude and orientation of the axial EMFs are shown schematically in Fig. 1. In the case of a DW with $w = 100$ nm and $V_{\text{DW}} = 100$ m/s in a magnetic WSM with $v_F = 10^6$ m/s and $JM_0 = 100$ meV, the strength of the axial fields at the center of the DW are given by $|\mathbf{E}_5| = 1$ V/cm and $|\mathbf{B}_5| = 1$ T.

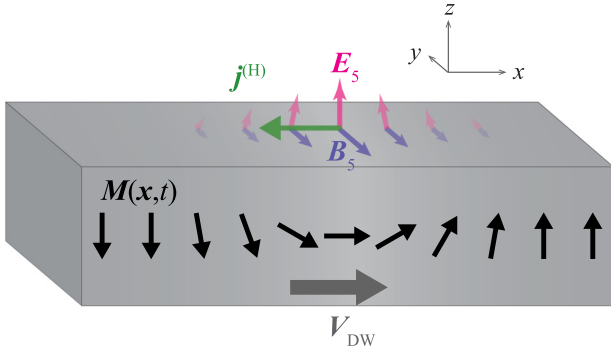


FIG. 1. Schematic showing the axial EMFs (E_5, B_5) and the induced Hall current $j^{(H)}$, along with a Néel domain wall moving with velocity V_{DW} .

Then, using the axial EMFs presented above and assuming that the chemical potential μ is slightly above the point of charge neutrality so that the quantum limit is valid, the regular Hall current corresponding to the charge-pumping effect can be estimated from Eq. (6) to find

$$\mathbf{j}^{(H)} = -\frac{e}{2\pi^2} \frac{JV_{\text{DW}}\mu}{v_F^2 w} [|\mathbf{M}'_{\perp}| \mathbf{e}_x + M'_x (\mathbf{e}_x \times \hat{\mathbf{B}}_5)], \quad (13)$$

where $\mathbf{M}_{\perp} = (0, M_y, M_z)$. The first term in the above equation represents the longitudinal current flowing along the moving DW, while the second term is the transverse current flowing parallel to the DW, which is independent of (y, z) and does not affect the charge conservation relation [Eq. (8)] since it is divergence-free. From this, we see that the charge pumping predominantly occurs close to the DW center, where the most drastic variation in $\mathbf{M}_{\perp}(x, t)$ occurs.

The amount of electric charge pumped along with the DW can be derived from the induced current using the charge conservation relation. Since both of the DW's x and t dependences are characterized by a single variable $\xi = (x - V_{\text{DW}}t)/w$, the differential operators on both sides of Eq. (8) are easy to treat, and lead to the charge distribution

$$\rho_{\text{pump}}(x, t) = \frac{1}{V_{\text{DW}}} j_x^{(H)}(x, t) = -\frac{e}{2\pi^2} \frac{J\mu}{v_F^2 w} |\mathbf{M}'_{\perp}|. \quad (14)$$

The net amounts of charge per unit area pumped by Néel and Bloch DWs are then given by

$$q_{\text{pump}}^{(\text{Néel})} = -\frac{e}{\pi^2} \frac{JM_0}{v_F^2} \mu, \quad q_{\text{pump}}^{(\text{Bloch})} = -\frac{e}{2\pi} \frac{JM_0}{v_F^2} \mu, \quad (15)$$

respectively. These net charges are independent of the DW width w , which implies that the charge pumping is indeed a topological effect. Moreover, in the case of the Néel wall, $q_{\text{pump}}^{(\text{Néel})}$ successfully accounts for the same amount of localized charge obtained by exactly counting the number of

bound states that was presented in previous work [17], which provides a guarantee of the validity of the quantum limit employed in this work.

The charge-pumping picture presented here can be used for any other type of DW, as long as the DW texture is sufficiently sharp so that the quantum limit approximation can be applied. As the pumping current discussed here can be effectively described as a quantum Hall effect, it is free from energy loss by Joule heating and thus distinct from the drift current arising from the spin motive force. Moreover, in a magnetic WSM, a conduction current beyond the DW gets suppressed as long as the charge disorder in the system is weak enough, which is observed numerically in Ref. [46]. This is because an electron in a Weyl cone requires a large-momentum scattering or a spin-flip process to be transmitted beyond the DW, since the positions of the two valleys in momentum space are exchanged at the DW. Therefore, the pumping current $\mathbf{j}^{(H)}$ can be captured as a dissipationless current pulse, (ideally) without Joule heating from the conduction current.

V. CONCLUSION

We have discussed the relation between the dynamics of magnetic textures and charge pumping in magnetic WSMs. Since the coupling between the magnetization and Weyl electrons may be viewed in terms of an axial gauge potential, the curl and time derivative of the magnetic texture correspond to axial magnetic and electric fields, respectively. The main message of this work [Eqs. (6) and (9)] is that these axial EMFs give rise to a regular Hall current, which can be regarded as a pumping current induced by the dynamics of the background magnetic texture. If the spatial variation of the magnetic texture is sufficiently slow, the induced current can be described by semiclassical transport theory, whereas sharp variations yield a pumping current described by the quantum Hall effect. The charge-pumping effect implies that a certain amount of localized charge [Eq. (10)] is induced by the axial magnetic flux, i.e., the curl of the magnetic texture. Conversely, it also implies that a local electrostatic potential that alters the local charge distribution would induce a magnetic texture in a magnetic WSM. The induced pumping current is free from Joule heating in the bulk even in the presence of impurities, since it arises as a Hall current. On the other hand, the dynamics of magnetic textures might be affected by the impurities (e.g., pinning and depinning of DWs), which is beyond the scope of our analysis and is left for future work.

Recent experimental measurements find that the Heusler alloy $\text{Co}_3\text{Sn}_2\text{S}_2$ shows the ferromagnetic WSM phase, with the Fermi level in the vicinity of the Weyl points [12], which would be a good candidate material for observing the charge-pumping effect proposed in our analysis. Verifying the existence of such an effect remains an open

question and further microscopic calculations are required to confirm this proposal. Nevertheless, from a topological point of view, the proposed pumping current and localized charge are simple manifestations of the interplay between the real-space topology and its momentum-space counterpart, which can generally be traced back to Berry curvatures defined in the global phase space [47].

By considering the coherent motion of a magnetic DW in a WSM, we compare the pumped charge with the localized charge calculated in previous work by more direct methods [17] and show their equivalence. The idea of charge pumping obtained here is also applicable to all kinds of magnetic textures: magnetic skyrmions and monopoles, for instance, carry pointlike charge, whereas magnetic helices can be accompanied by arrays of localized charge, i.e., charge density waves. This concept may help us to design efficient spintronic devices that make use of magnetic textures in magnetic WSMs, such as in a magnetic racetrack [48], where the motion of a magnetic texture can be electrically detected as a current pulse and can thus be used to read out information from an array of magnetic textures.

While we only consider a minimal ferromagnetic toy model in this work, the concepts developed here could be extended to other examples of TRS-broken WSMs. One particular case of interest would be that of antiferromagnetic order in WSMs, as exhibited in Mn_3Sn [13,21–23], which may exhibit similar TRS breaking and axial vector potential effects to those presented here for ferromagnetic order. However, since the ordering is not necessarily characterized by a single order parameter, this case would require more detailed microscopic investigations to clarify the relationship between the antiferromagnetic order and the charge degree of freedom.

ACKNOWLEDGMENTS

Y. A. is supported by JSPS KAKENHI Grant Number JP17K14316. K. N. is supported by JSPS KAKENHI Grant Numbers JP15H05854 and JP17K05485.

-
- [1] I. Žutić, J. Fabian, and S. Das Sarma, Spintronics: Fundamentals and applications, *Rev. Mod. Phys.* **76**, 323 (2004).
 - [2] A. Brataas, G. E. W. Bauer, and P. J. Kelly, Non-collinear magnetoelectronics, *Phys. Rep.* **427**, 157 (2006).
 - [3] G. Tatara, H. Kohno, and J. Shibata, Microscopic approach to current-driven domain wall dynamics, *Phys. Rep.* **468**, 213 (2008).
 - [4] S. Maekawa, S. O. Valenzuela, E. Saitoh, and T. Kimura, *Spin Current* (Oxford University Press, Oxford, UK, 2012).
 - [5] D. C. Ralph and M. D. Stiles, Spin transfer torques, *J. Magn. Magn. Mater.* **320**, 1190 (2008).
 - [6] S. E. Barnes and S. Maekawa, Generalization of Faraday's Law to Include Nonconservative Spin Forces, *Phys. Rev. Lett.* **98**, 246601 (2007).
 - [7] S. M. Young, S. Zaheer, J. C. Y. Teo, C. L. Kane, E. J. Mele, and A. M. Rappe, Dirac Semimetal in Three Dimensions, *Phys. Rev. Lett.* **108**, 140405 (2012).
 - [8] X. Wan, A. M. Turner, A. Vishwanath, and S. Y. Savrasov, Topological semimetal and Fermi-arc surface states in the electronic structure of pyrochlore iridates, *Phys. Rev. B* **83**, 205101 (2011).
 - [9] A. A. Burkov and L. Balents, Weyl Semimetal in a Topological Insulator Multilayer, *Phys. Rev. Lett.* **107**, 127205 (2011).
 - [10] A. A. Zyuzin, S. Wu, and A. A. Burkov, Weyl semimetal with broken time reversal and inversion symmetries, *Phys. Rev. B* **85**, 165110 (2012).
 - [11] C.-X. Liu, P. Ye, and X.-L. Qi, Chiral gauge field and axial anomaly in a Weyl semimetal, *Phys. Rev. B* **87**, 235306 (2013).
 - [12] E. Liu, Y. Sun, L. Müeçhler, A. Sun, L. Jiao, J. Kroder, V. Süß, H. Borrmann, W. Wang, W. Schnelle, S. Wirth, S. T. B. Goennenwein, and C. Felser, Giant anomalous Hall angle in a half-metallic magnetic Weyl semimetal, arXiv:1712.06722.
 - [13] K. Kuroda, T. Tomita, M.-T. Suzuki, C. Bareille, A. A. Nugroho, P. Goswami, M. Ochi, M. Ikhlas, M. Nakayama, S. Akebi, R. Noguchi, R. Ishii, N. Inami, K. Ono, H. Kumigashira, A. Varykhalov, T. Muro, T. Koretsune, R. Arita, S. Shin, T. Kondo, and S. Nakatsuji, Evidence for magnetic Weyl fermions in a correlated metal, *Nat. Mater.* **16**, 1090 (2017).
 - [14] M. V. Hosseini and M. Askari, Ruderman-Kittel-Kasuya-Yosida interaction in Weyl semimetals, *Phys. Rev. B* **92**, 224435 (2015).
 - [15] H.-R. Chang, J. Zhou, S.-X. Wang, W.-Y. Shan, and D. Xiao, RKKY interaction of magnetic impurities in Dirac and Weyl semimetals, *Phys. Rev. B* **92**, 241103 (2015).
 - [16] Y. Araki and K. Nomura, Spin textures and spin-wave excitations in doped Dirac-Weyl semimetals, *Phys. Rev. B* **93**, 094438 (2016).
 - [17] Y. Araki, A. Yoshida, and K. Nomura, Universal charge and current on magnetic domain walls in Weyl semimetals, *Phys. Rev. B* **94**, 115312 (2016).
 - [18] A. G. Grushin, J. W. F. Venderbos, A. Vishwanath, and R. Ilan, Inhomogeneous Weyl and Dirac Semimetals: Transport in Axial Magnetic Fields and Fermi Arc Surface States from Pseudo-Landau Levels, *Phys. Rev. X* **6**, 041046 (2016).
 - [19] Z. Wang, M. G. Vergniory, S. Kushwaha, M. Hirschberger, E. V. Chulkov, A. Ernst, N. P. Ong, R. J. Cava, and B. A. Bernevig, Time-Reversal Breaking Weyl Fermions in Magnetic Heuslers, *Phys. Rev. Lett.* **117**, 236401 (2016).
 - [20] G. Chang, S.-Y. Xu, H. Zheng, B. Singh, C.-H. Hsu, I. Belopolski, D. S. Sanchez, G. Bian, N. Alidoust, H. Lin, and M. Z. Hasan, Room-temperature magnetic topological semimetal state in half-metallic Heusler Co_2TiX ($X=\text{Si, Ge, or Sn}$), *Sci. Rep.* **6**, 38839 (2016).
 - [21] J. Kübler and C. Felser, Weyl points in the ferromagnetic Heusler compound Co_2MnAl , *Europhys. Lett.* **114**, 47005 (2016).

- [22] H. Yang, Y. Sun, Y. Zhang, W.-J. Shi, S. S. P. Parkin, and B. Yan, Topological Weyl semimetals in the chiral antiferromagnetic materials Mn_3Ge and Mn_3Sn , *New J. Phys.* **19**, 015008 (2017).
- [23] N. Ito and K. Nomura, Anomalous Hall Effect and Spontaneous Orbital Magnetization in Antiferromagnetic Weyl Metal, *J. Phys. Soc. Jpn.* **86**, 063703 (2017).
- [24] D. I. Pikulin, A. Chen, and M. Franz, Chiral Anomaly from Strain-Induced Gauge Fields in Dirac and Weyl Semimetals, *Phys. Rev. X* **6**, 041021 (2016).
- [25] T. Schulz, R. Ritz, A. Bauer, M. Halder, M. Wagner, C. Franz, C. Pfleiderer, K. Everschor, M. Garst, and A. Rosch, Emergent electrodynamics of skyrmions in a chiral magnet, *Nat. Phys.* **8**, 301 (2012).
- [26] N. Nagaosa and Y. Tokura, Emergent electromagnetism in solids, *Phys. Scr.* **T146**, 014020 (2012).
- [27] N. Nagaosa and Y. Tokura, Topological properties and dynamics of magnetic skyrmions, *Nat. Nanotechnol.* **8**, 899 (2013).
- [28] A. A. Zyuzin and A. A. Burkov, Topological response in Weyl semimetals and the chiral anomaly, *Phys. Rev. B* **86**, 115133 (2012).
- [29] P. Goswami and S. Tewari, Axionic field theory of (3+1)-dimensional Weyl semimetals, *Phys. Rev. B* **88**, 245107 (2013).
- [30] A. A. Burkov, Topological response in ferromagnets, *Phys. Rev. B* **89**, 155104 (2014).
- [31] A. A. Burkov, Anomalous Hall Effect in Weyl Metals, *Phys. Rev. Lett.* **113**, 187202 (2014).
- [32] A vector with a *hat* denotes its unit vector, i.e., $\hat{X} = X/|X|$.
- [33] K.-Y. Yang, Y.-M. Lu, and Y. Ran, Quantum Hall effects in a Weyl semimetal: Possible application in pyrochlore iridates, *Phys. Rev. B* **84**, 075129 (2011).
- [34] A. Vilenkin, Equilibrium parity-violating current in a magnetic field, *Phys. Rev. D* **22**, 3080 (1980).
- [35] K. Fukushima, D. E. Kharzeev, and H. J. Warringa, Chiral magnetic effect, *Phys. Rev. D* **78**, 074033 (2008).
- [36] D. E. Kharzeev, L. D. McLerran, and H. J. Warringa, The effects of topological charge change in heavy ion collisions: “Event by event P and CP violation”, *Nucl. Phys. A* **803**, 227 (2008).
- [37] D. E. Kharzeev, The Chiral magnetic effect and anomaly-induced transport, *Prog. Part. Nucl. Phys.* **75**, 133 (2014).
- [38] S. Nandy, G. Sharma, A. Taraphder, and S. Tewari, Chiral Anomaly as the Origin of the Planar Hall Effect in Weyl Semimetals, *Phys. Rev. Lett.* **119**, 176804 (2017).
- [39] K. Taguchi and Y. Tanaka, Axial current driven by magnetization dynamics in Dirac semimetals, *Phys. Rev. B* **91**, 054422 (2015).
- [40] J.-H. Zhou, H. Jiang, Q. Niu, and J.-R. Shi, Topological invariants of metals and the related physical effects, *Chin. Phys. Lett.* **30**, 027101 (2012).
- [41] Z.-M. Huang, J. Zhou, and S.-Q. Shen, Topological responses from chiral anomaly in multi-Weyl semimetals, *Phys. Rev. B* **96**, 085201 (2017).
- [42] E. V. Gorbar, V. A. Miransky, I. A. Shovkovy, and P. O. Sukhachov, Origin of Bardeen-Zumino current in lattice models of Weyl semimetals, *Phys. Rev. B* **96**, 085130 (2017).
- [43] S. L. Adler, Axial-vector vertex in spinor electrodynamics, *Phys. Rev.* **177**, 2426 (1969).
- [44] J. S. Bell and R. Jackiw, A PCAC puzzle: $\pi^0 \rightarrow \gamma\gamma$ in the σ -model, *Nuovo Cimento A* **60**, 47 (1969).
- [45] H. B. Nielsen and M. Ninomiya, The Adler-Bell-Jackiw anomaly and Weyl fermions in a crystal, *Phys. Lett.* **130B**, 390 (1983).
- [46] K. Kobayashi, Y. Ominato, and K. Nomura, Helicity-protected domain-wall magnetoresistance in ferromagnetic Weyl semimetal, arXiv:1802.04536. *J. Phys. Soc. Jpn.* **87**, 073707 (2018).
- [47] D. Xiao, M.-C. Chang, and Q. Niu, Berry phase effects on electronic properties, *Rev. Mod. Phys.* **82**, 1959 (2010).
- [48] S. S. P. Parkin, M. Hayashi, and L. Thomas, Magnetic domain-wall racetrack memory, *Science* **320**, 190 (2008).